Met. Mater. Int., Vol. 21, No. 2 (2015), pp. 391~401
doi: 10.1007/s12540-015-4382-1

Effect of Processing Routes in a Multi-Pass Continuous Hybrid Process on Mechanical Properties, Microstructure, and Texture Evolutions of Low-Carbon Steel Wires

Sun Kwang Hwang[1], Hyun Moo Baek[2], Ho Seon Joo[3], and Yong-Taek Im[3,4,*]

[1]Ultimate Manufacturing Technology R&BD Group, KITECH, Daegu 711-883, Korea
[2]Land Systems Engineering Team, Changwon Regional Center, DTaQ, Changwon 642-160, Korea
[3]Department of Mechanical Engineering, KAIST, Deajeon 305-701, Korea
[4]Office of the President, KIMM, Daejeon 305-343, Korea

(received date: 14 August 2014 / accepted date: 23 September 2014)

In this work, a multi-pass continuous hybrid (CH) process was experimentally applied with up to five passes with three processing routes, A, B_c, and C, to check the practicality of the processing routes and investigate their effect on the mechanical properties, microstructure, and texture evolutions of low-carbon steel wires. According to the present investigation, the wires processed by the 5th pass CH process with route A showed the highest ultimate tensile strength value (762 MPa) compared to those for routes B_c (718 MPa) and C (720 MPa), respectively. Based on the compression test results, the CH processed wire showed good workability when the aspect ratio was smaller than 2.4 for all the processing routes. According to the microstructure and texture evolutions, the grain sizes of the 5th pass CH processed wires decreased for all the processing routes than that of the initial specimen, and the wires showed mixed texture distribution of shear and drawing texture components. From the present investigation, it was concluded that the processing routes of the CH process could strongly affect the microstructure and texture evolutions, resulting in changes of the mechanical properties and workability of the low-carbon steel wires.

Keywords: metals, deformation, mechanical properties, microstructure, texture

1. INTRODUCTION

In recent decades, the manufacturing of high-strength and high-durability materials such as wires, bars, and sheets by severe plastic deformation (SPD) processes [1-7] has become one of the most important issues in various industrial fields, such as transportation and construction, to save the energy and improve the quality of products. Of various steel wires, low-carbon steel wire is one of the common types of steel wire for general uses such as fasteners, nails, and industrial ropes. The wires are generally fabricated by a wire drawing process to satisfy the geometrical and structural demands.

However, it is not easy to meet industrial requirements using the conventional wire drawing process only since the process in its original design has a limitation in that it applies large plastic deformation to the material. In this regard, several processes have been developed to manufacture high-strength wires more efficiently compared to the conventional wire drawing process. Chakkingal *et al*. [8,9] developed an equal channel angular drawing (ECAD) by drawing a specimen through a die consisting of two channels of equal cross-section intersecting at an angle, generally between 90° and 150°. According to the work by León and Luis [10], the ECAD process could impose higher plastic deformation on the specimen than the conventional wire drawing process for the same area reduction. In addition, Hwang *et al*. [11] numerically and experimentally investigated a multi-pass shear drawing (SD) process to secure stable flow and impose high plastic deformation on the specimen as a continuous process at room temperature. These two processes were mostly designed by applying simple shear deformation into the specimen, resulting in grain refinement in the steel wire. However, the ECAD and SD processes could not achieve a significant increase in the mechanical strength of the processed wire compared to the conventional wire drawing process because the shear deformation was not large enough to efficiently incur the grain refinement in the wire.

Hwang *et al*. [12] proposed a non-circular drawing (NCD) sequence, which could produce high-strength wires compared to the conventional wire drawing process for industrial applications. Furthermore, Lee *et al*. [13] experimentally car-

*Corresponding author: ytim@kaist.ac.kr, ytim@kimm.re.kr

ried out the NCD sequence up to the 10th pass with low-carbon steel wires. According to their results, high-strength low-carbon steel wires with relatively better ductility could be manufactured by the NCD sequence, resulting in grain refinement in the processed specimen compared to the conventional wire drawing process. However, after the 8th pass, the ultimate tensile strength (UTS) value of the wire processed by the NCD sequence was lower than that of the wire drawing process owing to the increased Bauschinger effect. Recently, Hwang *et al*. [14,15] proposed a continuous hybrid (CH) process to manufacture the wires with enhanced mechanical properties for industrial applications and also extended the process to a pilot case study for a single pass. They reported that the process could be beneficial in commercializing a continuous process for various industrial applications. The CH process was additionally investigated by Kim *et al*. [16] for up to two passes to produce high-strength bolts using the fine-grained AA6061-O wire at room temperature. They reported that the CH process could be applied for manufacturing wires continuously to efficiently produce high-strength parts. The multi-pass CH process was numerically and experimentally carried out with route A at room temperature by Hwang *et al*. [17] to study the effect of grain-refinement microstructure on mechanical properties and fatigue limit values of low-carbon steel wires. According to this work, it was found that the multi-pass CH process might be more efficient in manufacturing high-strength and high-durability wires compared to the conventional wire drawing process.

The mechanical properties and workability of the specimen are strongly related to the microstructure and texture evolution of the processed specimen by cold metal forming. According to a study by Ito and Horita [18], the change in mechanical properties was attributed to microstructure evolution, such as accumulation of dislocations, and to the formation of grain boundaries. In addition, Sugondo *et al*. [19] found that there was a strong texture build-up of the <110> fiber component in the body-centered cubic (BCC) material during the wire drawing process, which improved the cold forgeability of the wires. In particular, an equal channel angular pressing (ECAP) originally introduced by Segal [20] is well known as an effective technique for producing ultra-fine grained materials by controlling microstructure and texture evolution efficiently. According to the literature [21], the processing methods in the ECAP can be typically defined as three processing routes, A, B_c, and C, in that order. In routes A, B_c, and C, the specimen was re-inserted in the ECAP dies with rotations of 0°, 90°, and 180°, respectively, during the multi-pass process. Choi *et al*. [22,23] investigated the effect of processing routes in the ECAP process on the workability of the commercially-available aluminum alloys of AA1050 and AA6061, respectively. According to their research, different microstructure evolutions were seen depending on the processing routes during the multi-pass ECAP, resulting in different mechanical properties and workability characteristics of the processed specimen. In this regard, most material behavior cannot be fully understood without investigating the microstructure and texture evolutions.

In this work, the multi-pass CH process was experimentally investigated and applied with up to five passes to check the effect of processing routes on the mechanical properties, workability, microstructure, and texture evolutions of low-carbon steel wires. In the multi-pass CH process, three processing routes consisting of routes A, B_c, and C were introduced. To evaluate the mechanical properties of the processed wires, tension and Vickers micro-hardness tests were carried out for comparisons among three processing routes, respectively. A compression test was also conducted to check the workability of the wires processed by the CH process for each processing route. Microstructure and texture evolutions of the wires were also investigated by introducing the optical microscopy (OM), electron backscattering diffraction (EBSD), transmission electron microscopy (TEM), and X-ray diffraction (XRD).

2. EXPERIMENTAL PROCEDURE

In the present investigation, commercially-available low-carbon steel with the chemical composition (C 0.08-0.13, Si 0.10, Mn 0.30-0.60, P 0.03, S 0.03, and Al 0.02 in weight percent) was used for the CH process. To straighten out the specimen prepared by a coiling process, a coil with an initial diameter of a 14 mm was drawn to the diameter of a 13 mm wire by a single-pass wire drawing process. The straightened wires were annealed at 900 °C for 1 h and air cooled to room temperature to remove previous deformation and thermal history. After that, acid pickling was applied for removing scale from the annealed wires before carrying out the experiments.

The multi-pass CH process with processing routes A, B_c, and C was designed and applied with up to five passes and 20% area reduction for each pass at room temperature to investigate the effect of the processing routes on the deformation behavior during the process. In routes A, B_c, and C, the specimen was re-inserted in the ECAP die with rotations of 0°, 90°, and 180° after each pass, respectively, as shown in Fig. 1. A reference system of the CH process is referred to as transverse direction (TD), normal direction (ND), and exit direction (ED).

Figure 2 shows the experimental set-up and dies for the CH process used in the present study available at POSCO Technical Research Laboratory. The material flow of the processed wire was controlled by the rolls and grip. The velocities of the rolls and grip applied for the CH process were 0.047 rad/s and 10 mm/s, respectively. During the CH process, the wire passed through the rolls, ECAP, and wire drawing dies in sequence. In this work, the same dies used for the previous work by Hwang *et al*. [17] were employed. The integral

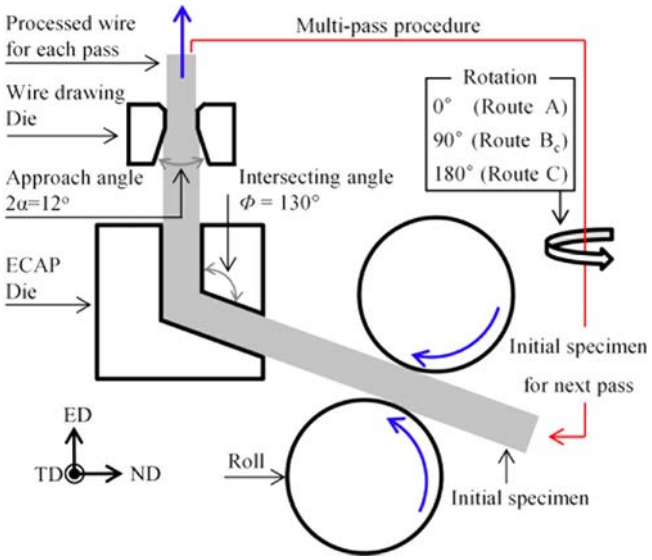

Fig. 1. Schematic diagram of the CH process and its processing routes during the multi-pass procedure.

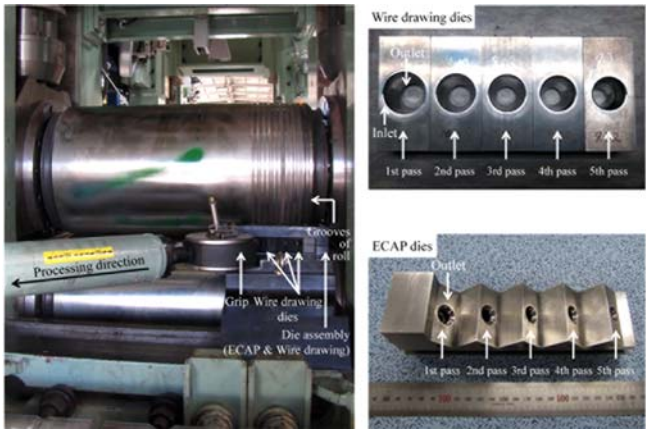

Fig. 2. Experimental set-up of the CH process and the dies used in experiments.

ECAP dies with an intersecting angle (Φ) of 130° were used up to the 5th pass process, as shown in Fig. 2. The wire drawing dies with the internal geometry of an approach angle (2α) of 12° were used as well. Commercially-available liquid lubricant (Aim Cut 1004A) was applied between the wire and dies to minimize the frictional force, while the lubricant was not used on the rolls in order to impose high frictional force on the wire during the CH process.

Tension tests were conducted to investigate the mechanical property changes such as the UTS, elongation at fracture, and static toughness of the processed wires for various processing routes. Figure 3(a) shows the dimension of the specimens used in the tension test. It was machined off from the processed wires according to ASTM Standard [24]. Tension tests were carried out twice for each condition using an Instron 5583 with a constant crosshead speed of 0.017 mm/s, which corresponds to an initial strain rate of 6.7×10^{-4} s^{-1} at room temperature. During the tests, elongation was calculated by a mechanical extensometer (Instron 2630-100 series, clip-on type) with a gauge length of 25 mm. The static toughness of the wire was measured by integrating the area of the engineering stress-strain curves obtained by the tension test.

Vickers micro-hardness tests were also carried out to examine the local strength distribution of the processed wires during the CH process. The specimens were cut in parallel to the ED plane and the cross-section of the specimen was cold mounted and mechanically polished up to 1 μm by SiC papers and diamond suspensions. Vickers micro-hardness values were measured by Mitutoyo HM-122 at 21 points at regular intervals along the line, excluding 0.2 mm at both ends of the specimen. Figure 3(b) shows the data acquisition line for the Vickers micro-hardness test. The applied load was 1.96 N, and the duration was 10 s.

Compression tests were conducted with a 100 kN MTS machine (Alliance RT/100) at room temperature to check the workability of the initial and processed wires by the CH process for various processing routes by simple visual inspection of the compressed specimen even though further investigation might be required to obtain accurate data considering texture-induced anisotropy. Specimens for the test were made into a cylindrical shape of 4 mm in diameter and various heights from 8.8 to 11.2 mm. Tungsten carbide platens equipped with the guide post apparatus were used, as shown in Fig. 4. A compression test was applied with a ram speed of 0.1 mm/s, and grease was applied between the specimen and the platens

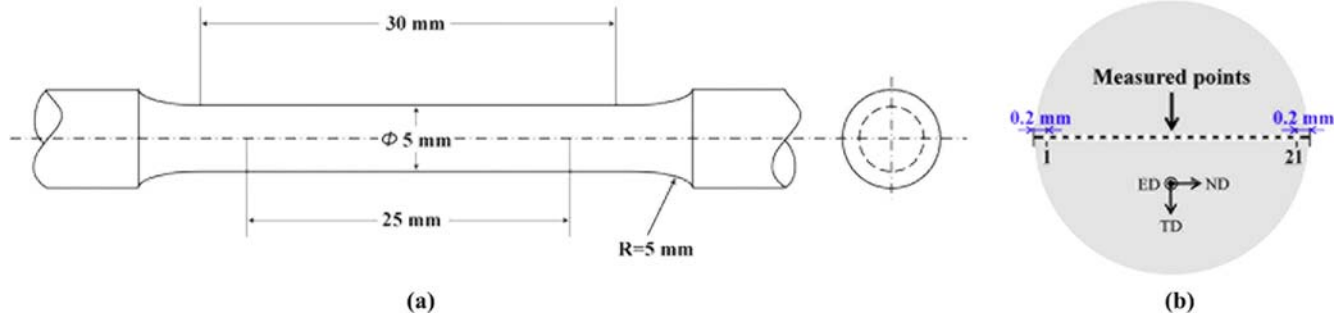

Fig. 3. (a) Dimension of the specimens for the tension test and (b) the data acquisition line for the Vickers micro-hardness test.

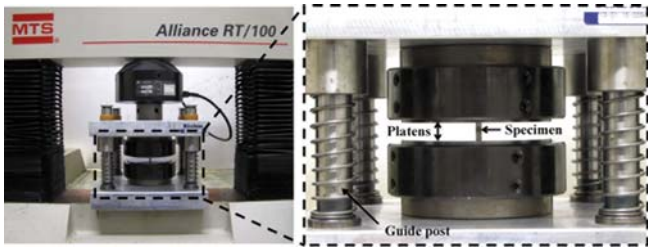

Fig. 4. Experimental set-up of the compression test.

as lubricant. The height of the compressed specimen was measured to calculate the compressive strain, as described in Eq. (1):

$$\varepsilon = \ln\left(\frac{h_i}{h_f}\right), \quad (1)$$

where h_i and h_f are the initial and final heights of the specimen, respectively. The experiments were carried out until the compressive strain of the deformed specimen was 1 for each specimen to impose sufficient plastic deformation. To obtain reproducible data, the tests were conducted twice for the same experimental conditions.

To observe the microstructure and texture evolution by the OM, EBSD, and XRD, the wires processed by each processing route were sliced into two at the middle part in parallel to the TD plane. The sliced specimens were cold mounted and mechanically polished up to 1 μm by SiC papers and diamond suspensions to obtain a clean and smooth surface.

The prepared specimen was additionally etched with 2% nital solution to investigate the microstructure evolution of the processed wires using Olympus BX51 with 200 times magnifications for obtaining the OM images.

To check microstructural change by the EBSD, the samples were prepared by additional polishing using colloidal silica solution with a duration of 20 min in order to make the surface of the specimen stress-free. The EBSD was obtained at the central region of each sample by using EDAX-TSL/Hikari attached to a field emission scanning electron microscope (FE-SEM, Hitachi SU6600). Measurement conditions of an accelerated voltage of 20 kV, specimen tilt of 70°, and scan step size of 0.08 μm were used. Each scan covered an area of 30 μm × 80 μm. The EBSD data was post-processed by commercial software (TSL OIM Analysis 6.13). For clean-up procedures, grain confidence index standardization and grain dilation with their default parameters and single iteration were used for the collected data points with a confidence index greater than 0.1. In the EBSD results, the average grain size of the diameter was calculated by the area fraction method (EDAX, TSL Crystallography Orientation Imaging Microscopy) to estimate the grain sizes of the wires processed by the 5th pass CH process for three processing routes.

200 kV FE-TEM (JEOL JEM-2100F HR) was used to investigate the microstructure change of the wire processed by the 5th pass CH process with three processing routes. The samples were prepared at the center of the processed wire by using a focused ion beam (FIB, Hitachi FB-2100) in parallel to the TD plane.

To investigate the texture evolution of the processed wires, XRD (Rigaku D/MAX-2500) was employed in the present work. The 2θ scan range was measured from 40° to 90° at a step size of 0.01° and a speed of 4°/min. The Cu Kα radiation was used with generator settings of 40 kV and 300 mA. The pole figures (PFs) for (110), (200), and (211) in the ferrite phase were obtained and corrected for background and defocussing. To calculate the orientation distribution functions (ODFs) and quantitative texture components, incomplete PFs were used. And then, complete PFs were recalculated from ODFs using commercially-available texture analysis software (LaboTex 3.0).

3. RESULTS AND DISCUSSION

Figure 5 shows the engineering stress-strain curves, UTS, elongation at fracture, and static toughness values obtained from the tension tests for the initial and produced wires by the CH process for the various passes and processing routes. The mechanical property values obtained from the curves are summarized in Table 1. The UTS value of the initial specimen was 376 MPa. After the 1st pass CH process, the value increased up to 603 MPa. The UTS values of the wires produced by the CH process for all the passes and processing routes were higher than that of the initial specimen. After the 5th pass, the UTS values of the processed wire by routes A, B_c, and C became 762, 718, and 720 MPa, respectively. That is, the UTS values of the wires produced by the 5th CH process with A, B_c, and C were 102.7%, 91.0%, and 91.5% higher, respectively, compared to that of the initial specimen. In addition, the wire produced by the CH process with route A showed 6.1% and 5.8% higher UTS value than those for routes B_c and C, respectively. The value (739 MPa) of the wire produced by the 4th pass CH process with route A was higher than the values of wires produced by the 5th pass with routes B_c and C, respectively.

The elongation at the fracture and static toughness values of the produced wires by the CH process significantly decreased for all of the passes compared to those of the initial specimen while the mechanical strength of the wires increased, as shown in Fig. 5. This is a general characteristic of material processing deformed by cold forming process. The elongation and toughness values of the initial specimen were 41.2% and 141.3 x 10^6 J/m^3, respectively. After the 1st pass, these values became 11.1% and 55.3 x 10^6 J/m^3, respectively. Interestingly, the elongation showed similar values (9.6~10.2%) up to the 5th pass for all the processing routes, resulting in an increase of the toughness value compared to that of the 1st pass due to enhancement of mechanical strength. In particu-

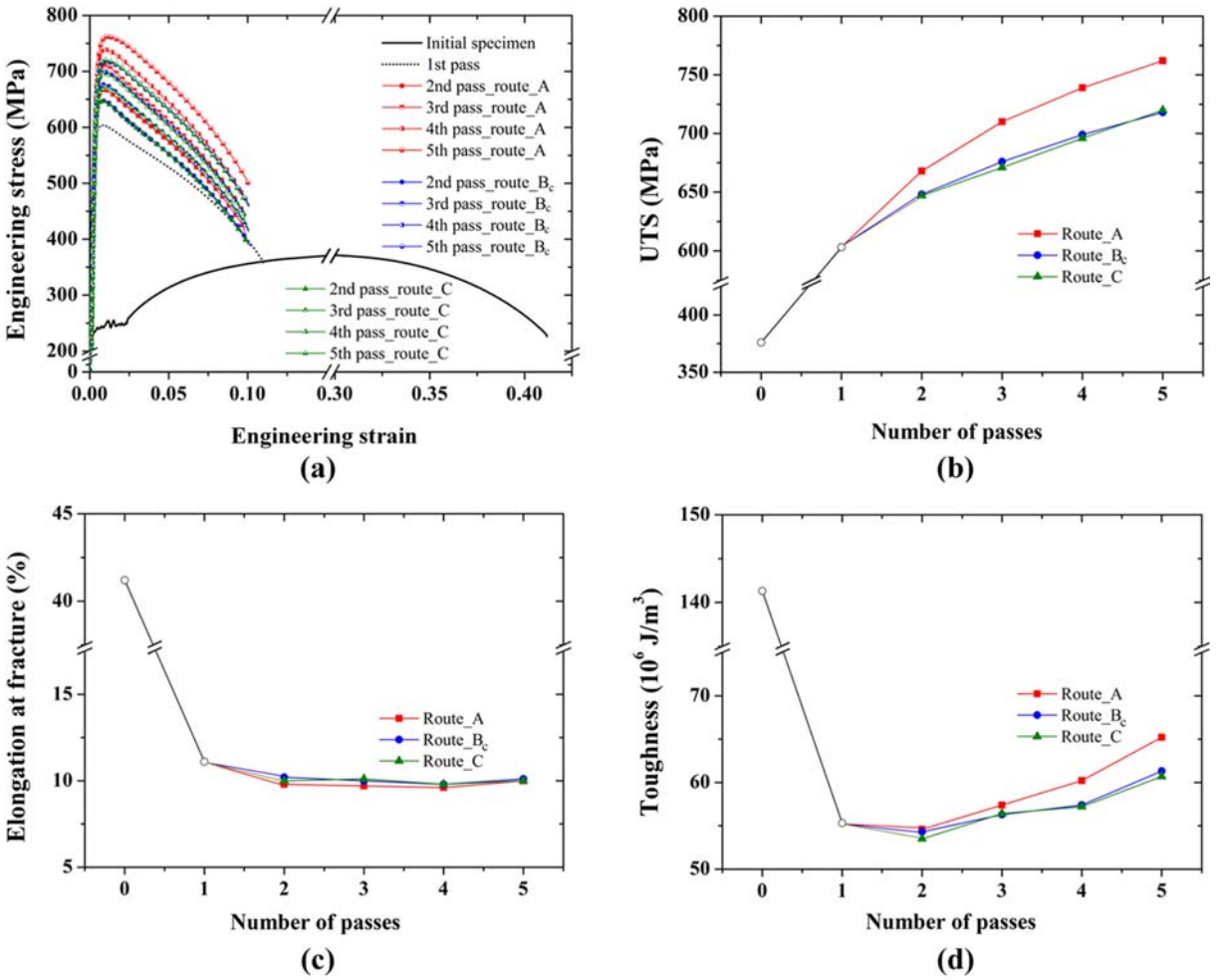

Fig. 5. (a) Stress-strain curves and (b) UTS, (c) elongation at fracture, and (d) toughness obtained from the tension tests for the initial and processed wires by the CH process for various processing routes and passes.

Table 1. Mechanical properties obtained from the tension tests of the initial and produced wires by the CH process for various processing routes and passes

Specimen	Processing route	No. of passes	UTS (MPa)	Elongation at fracture (%)	Toughness (10^6 J/m^3)
Initial	-	0	376	41.2	141.3
CH	-	1	603	11.1	55.3
	A	2	668	9.8	54.6
		3	710	9.7	57.4
		4	739	9.6	60.2
		5	762	10.0	65.2
	B_c	2	648	10.2	54.3
		3	676	10.0	56.3
		4	699	9.8	57.4
		5	718	10.1	61.3
	C	2	647	10.0	53.5
		3	671	10.1	56.4
		4	696	9.8	57.2
		5	720	10.0	60.7

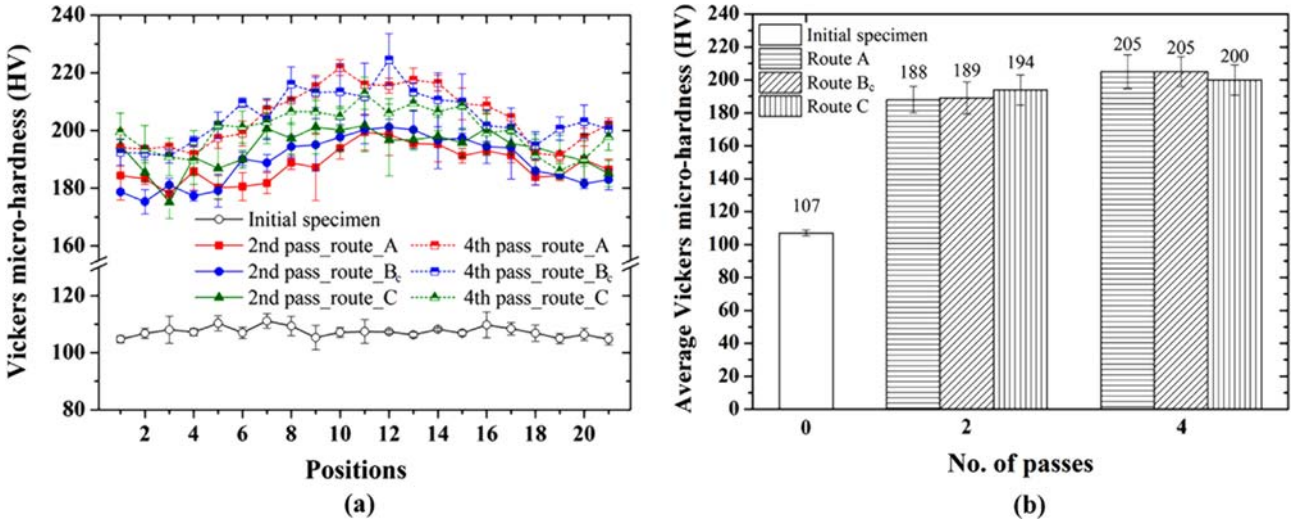

Fig. 6. (a) Distributions of the measured Vickers micro-hardness with a standard deviation and (b) their average values.

lar, the toughness value of the wires processed by route A was higher than those for other processing routes for all the passes. From these investigations, it was found that the CH process, especially route A, could manufacture high-strength low-carbon steel wires with higher static toughness among three processing routes.

Figure 6 shows the distributions and average hardness values obtained from the Vickers micro-hardness test. According to the test results, for the wires produced by the CH process for each pass, micro-hardness distributions were relatively non-uniform compared to that of the initial specimen due to accumulation of plastic deformation on the wire by the friction effect and die geometry of the process. However, the difference of the micro-hardness value among three processing routes for each pass was less than about 3%. The Vickers micro-hardness value clearly increased from the data obtained from the initial specimen depending on the applied level of plastic deformation. The average micro-hardness values obtained from the wire produced by the 2nd and 4th pass CH process for all processing routes increased by about 80% and 90%, respectively, compared to that of the initial specimen. From these results, the CH process could manufacture low-carbon steel wires with enhanced micro-hardness values compared to the initial specimen for all the processing routes without a large difference of standard deviation.

Figure 7 shows the compression test results for the initial and processed wires by the multi-pass CH process with the various processing routes. According to the results, buck-

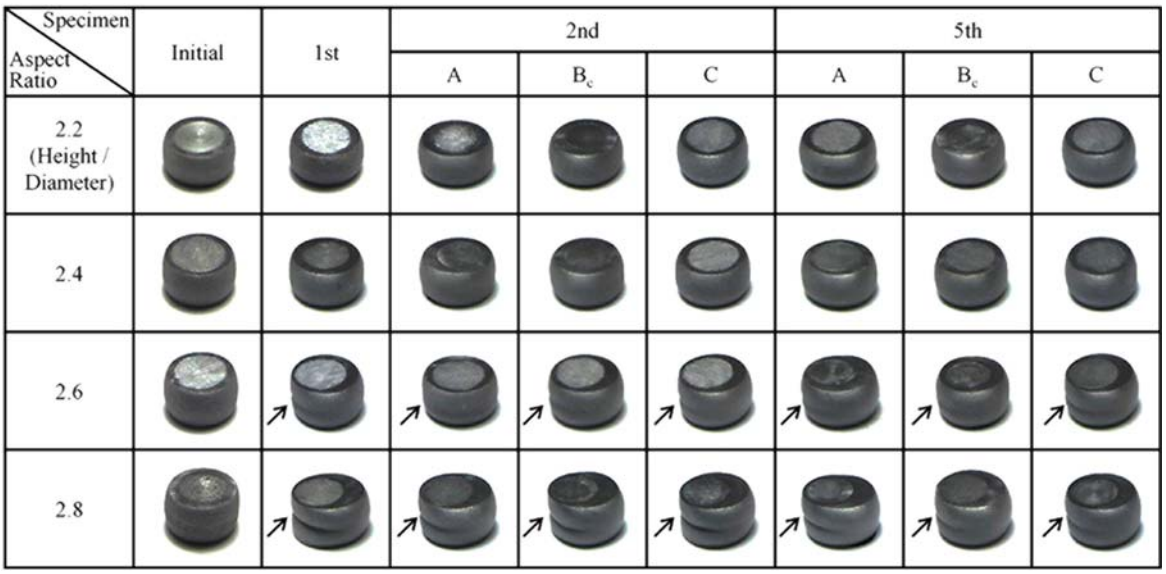

Fig. 7. Results of the compression test (The arrows indicate the occurrence of buckling).

ling did not occur for all the aspect ratios of the height to the diameter for the initial specimen. On the other hand, the produced specimens by the CH process buckled when the aspect ratio was larger than 2.6 for all processing conditions. According to the works by Choi *et al*. [23], the reason for this different critical aspect ratio was due to the shear plane, which was related to the die intersecting angle of the ECAP die, and route effect during the ECAP process. This directionality might cause microstructure and texture evolutions, resulting in buckling along the shear direction. Therefore, wires produced by the CH process require a careful control of the microstructure and texture evolutions to achieve sufficient workability for various industrial applications. In this study, it was concluded that the aspect ratio of the produced low-carbon steel wires by the multi-pass CH process with the 130° intersecting angle of the ECAP die should be selected smaller than 2.4 to guarantee safe workability.

Figure 8 shows the microstructure distribution observed by the OM for the initial and produced wires by the 1st pass [15] and 2nd pass CH process with routes A and C, respectively. The microstructure of the initial specimen showed equiaxed ferrite grains. According to the previous work by Hwang *et al*. [15], the microstructure evolution of the produced wire by the CH process for the 1st pass was inclined and elongated along the shear plane of the ECAP dies. After the 2nd pass, different microstructure evolutions in the deformed wires were observed between processing routes A and C. The wire produced by the 2nd pass CH process with route A showed more elongated and inclined microstructure along the ED compared to that by the 1st pass CH process while route C showed equiaxed grains similar to the initial microstructure, as described in the schematic illustration in Fig. 8. According to the investigations of the shearing characteristics in the conventional ECAP process by Furukawa *et al*. [21] and Fukuda *et al*. [25], route A led to shearing on the different slip plane at each pass and thus the grains were more elongated and inclined along the ED as the number of passes increased. On the other hand, route C led to repetitive shearing on the same slip plane in the opposite direction for each pass. Therefore, the grain was restored to the equiaxed one after every even pass, which was similar to the initial microstructure. From these observations, it was concluded that the microstructure evolution of the multi-pass CH process was affected by the processing routes due to the different shear plane between routes A and C, as shown in Fig. 8.

In the EBSD data presented in Fig. 9, low angle grain boundaries (LAGBs) ($2° \le \theta < 15°$) are shown as red lines, and high angle grain boundaries (HAGBs) ($15° \le \theta$) are shown as blue lines. The initial microstructure consisted of equiaxed grains, similar to the above-mentioned OM results, with almost all grains surrounded by HAGBs, as shown in Fig. 9(a). After the 5th pass, the formation of LAGBs increased explosively grown for all the processing routes due to accumulation of dislocations by the plastic deformation while the LAGBs were rarely seen in the initial specimen. According to the work by Ito and Horita [18], the grain refinement mechanism followed dislocation accumulation, formation of LAGBs, increase of misorientation angles, absorption of dislocations at HAGBs, and establishment of a steady state. From this grain refinement mechanism, formation of LAGBs led to grain refinement of the processed specimen by the 5th pass CH process for all the processing routes compared to the initial one, as shown in Fig. 9.

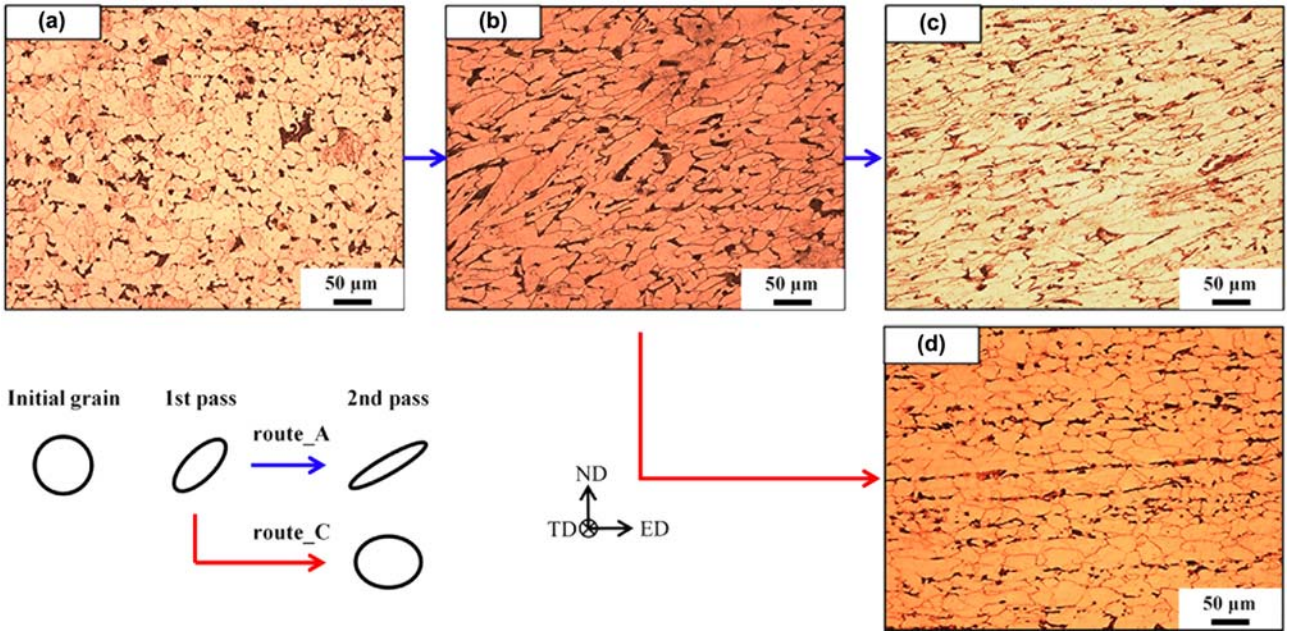

Fig. 8. OM images: initial and processed wires by the 1st pass [15] and 2nd pass CH process with routes A and C, respectively. (a) Initial, (b) 1st, (c) 2nd_A, and (d) 2nd_C.

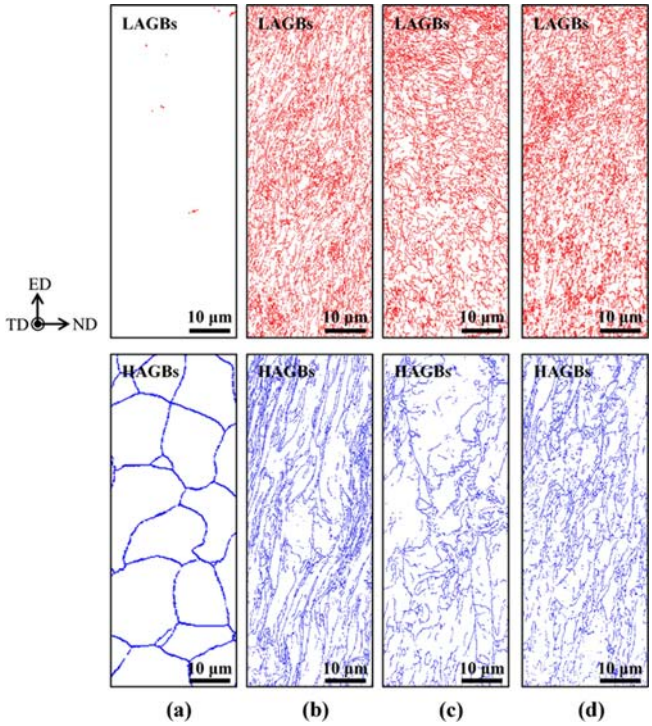

Fig. 9. EBSD maps: evolution of LAGBs ($2° \le \theta < 15°$, red lines) and HAGBs ($15° \le \theta$, blue lines): the specimen of (a) the initial and 5th pass CH process with routes (b) A, (c) B_c, and (d) C, in that order.

From the obtained EBSD data, the average grain size calculated for the initial specimen was 20.05 μm. The grain sizes of the wires produced by the 5th pass CH process for all the processing routes decreased compared to that of the initial specimen. In particular, the average grain size (3.02 μm) of the specimen processed by route C was smaller than those (4.29 μm and 6.71 μm) for the processed wires by routes A and B_c, respectively.

According to previous works, route A of ECAP is an effective processing route for grain refinement of fcc metals compared to route C [26,27]. However, the most effective ECAP route for the grain refinement is still controversial because some references have reported that route B_c or C might be better than route A, depending on the material and intersecting angle of the ECAP die [21,28]. According to the work by Zhu and Lowe [29], the intersection of the shear plane and crystal structures plays a primary role in the grain refinement of the processed material by ECAP. They reported that route C was found to be more effective in grain refinement than route A for an intersecting angle of 90°, but less effective than route A for an intersecting angle of 120°. These tendencies agreed well with fcc metals such as aluminum and copper, as well as hcp metals, but might not work for bcc metals. Therefore, route C of the CH process with the 130° intersecting angle of the ECAP die for the low-carbon steel might be one such case. In addition, the CH process combined with

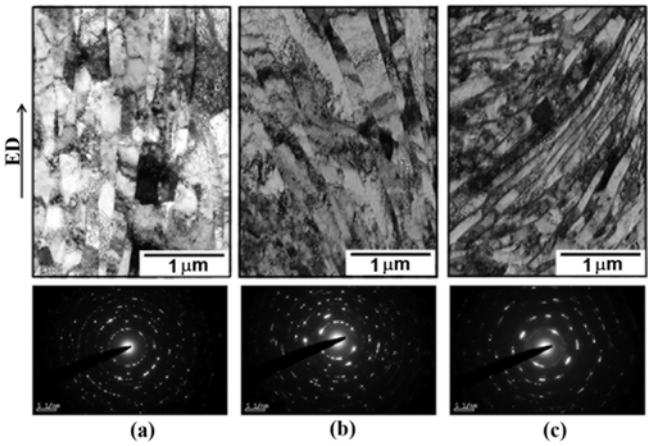

Fig. 10. TEM images obtained from the wires processed by the 5th pass CH process with routes (a) A, (b) B_c, and (c) C, in that order.

rolling, ECAP, and drawing processes in sequence might lead to newly activated slip systems during the process, resulting in different strain paths than with the conventional ECAP.

Figure 10 shows the microstructure evolution measured by the TEM for the 5th pass CH process at the various processing routes. The initial grains were divided, and many dislocations were observed within the grains owing to the accumulation of high plastic deformation. In particular, the specimen produced by route C showed the smallest deformation bands (less than 1 μm) among the various processing routes similar to the above-mentioned EBSD results. The continuous circular patterns with diffracted beams are seen in the selected area electron diffraction. According to the work by Fukuda *et al*. [25], the patterns show that there are potentially many sub- or refined-grains with boundaries having high angles of misorientation within the aperture size area. From the investigation of microstructure evolution by the EBSD and TEM, it was found that the multi-pass CH process can be effective in producing fine-grained wires. In particular, among the various processing routes, route C could manufacture the smallest grains during the multi-pass CH process.

Texture evolutions of the initial and drawn wire by the different processing routes are presented in terms of PFs and ODFs. Figure 11 shows the (110) PFs measured by the XRD for the initial and processed wires. The initial specimen showed random texture except for the central part of the specimen, in which high pole intensity existed after an annealing of 900 ℃ for 1 h and air cooling to room temperature to remove previous deformation and thermal history. The PFs of the wire produced by the 1st pass CH process represent the combination of the ECAP and wire drawing textures. According to the previous work by Hwang *et al*. [15], the PFs of the wires produced by the CH process showed mixed texture evolution of shear texture by the ECAP and drawing texture by the wire drawing due to combination of shear and draw-

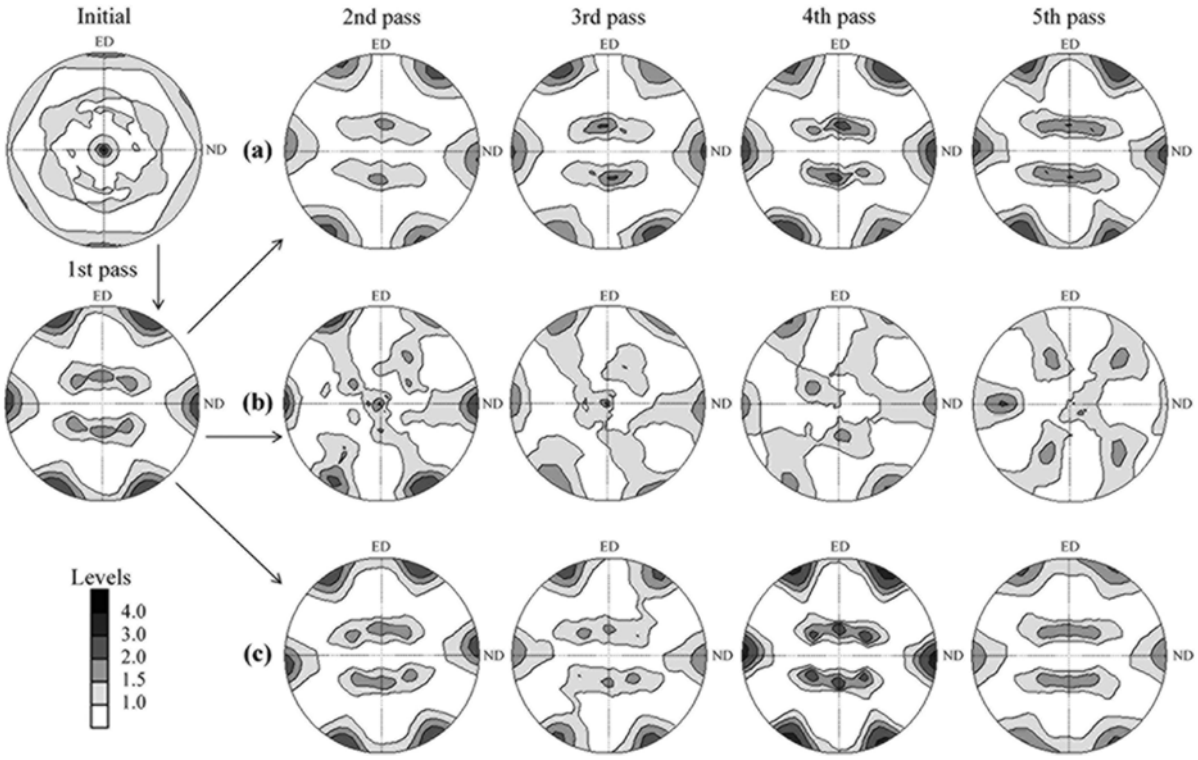

Fig. 11. (110) PFs: specimens processed by routes (a) A, (b) B_c, and (c) C, in that order.

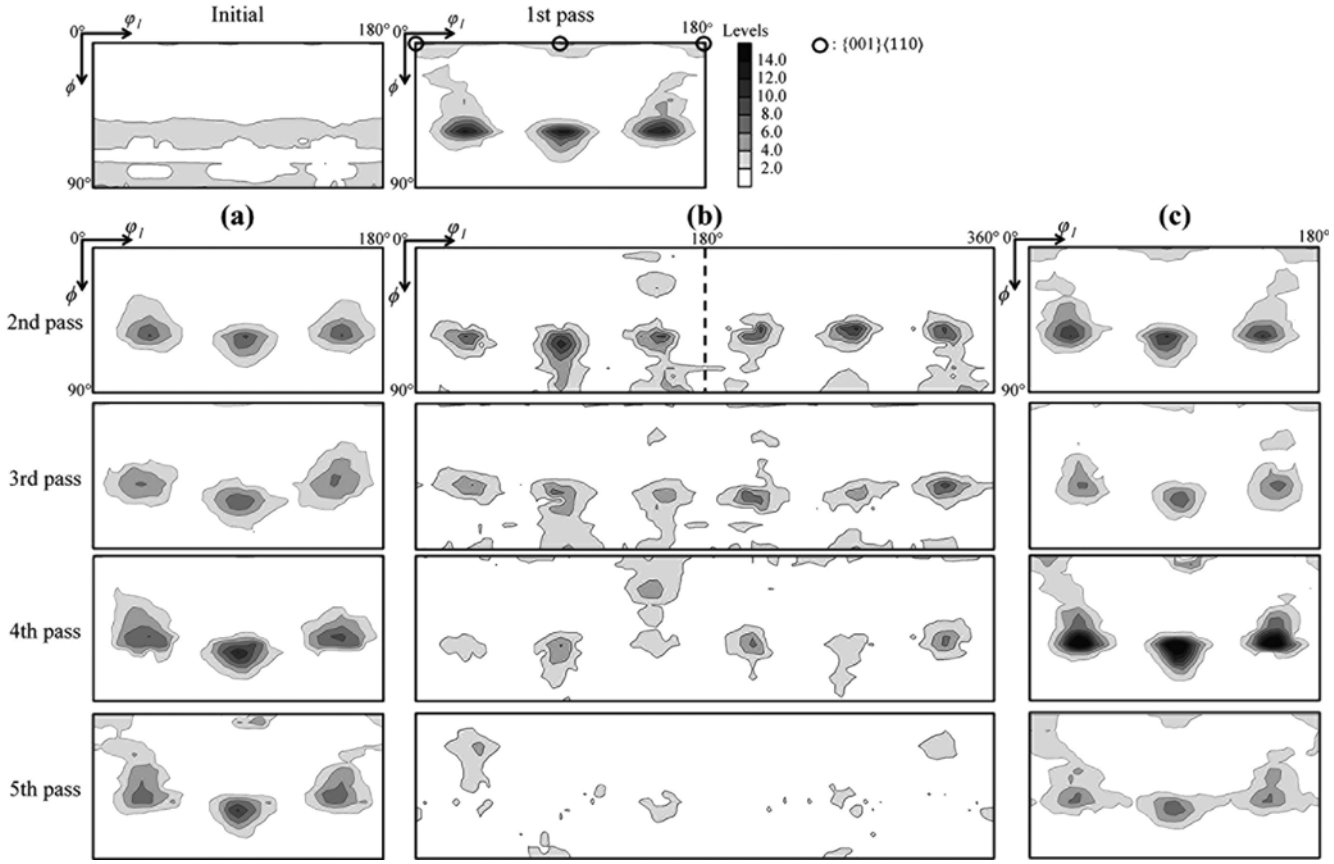

Fig. 12. ODFs: specimens processed by the multi-pass CH process with (a) routes A, (b) B_c, and (c) C, in that order.

ing deformation modes involved with the process. During the multi-pass CH process, the texture evolution was dependent on the processing routes and number of passes. The PFs of the processed specimens by routes A and C up to the 5th pass were roughly similar to those for the 1st pass. Interestingly, the texture intensity of the specimen did not regularly change during the multi-pass CH process. Generally, the shear texture intensity of the specimen processed by the conventional ECAP with route A increased with the number of passes. In this study, however, the specimen produced by the CH process with route A did not show a regular increase of the texture intensity during the multi-pass CH process. Because the CH process consists of the rolling, ECAP, and wire drawing processes, an increase of simple shear texture intensity was rarely observed during the process. In addition, the specimen processed by route B_c showed relatively different texture evolution compared to those for other routes.

Figure 12 also shows the deformation textures of the ODFs plots (φ_2= 45°) for the initial and produced specimens by the CH process with the various processing conditions, respectively. The ODFs plots can separate the overlapped components in the PFs, allowing for more clear comparison of the individual components. The texture for routes A and C showed monoclinic sample symmetry, and a range of φ_1=0~180° was used in the plots while that for route B_c was triclinic (φ_1=0~360°).

The texture of the specimen produced by the CH process for the 1st pass showed a combination of the shear and drawing textures. In particular, the components of {001}<110> in the wire drawing texture were observed, as shown in this figure. During the multi-pass CH process, deformation textures observed in the ODFs plots were similar to the PFs results. The processed specimens by routes A and C showed similar texture evolution while the texture intensity was slightly changed during the process. Interestingly, the texture intensity of the specimen processed by route B_c gradually decreased up to the 5th pass. One explanation might be that the deformation texture of the specimen by route B_c was gradually weakened compared to the previous one because the specimen was inserted in the rolling, ECAP, and wire drawing dies in sequence with rotation of 90° after each pass. From these investigations, the CH process could control the deformation texture by the processing passes and routes, respectively, resulting in the mechanical property changes and workability changes.

4. CONCLUSIONS

Based on the experimental results of the present investigation, the following conclusions are derived:

(1) The UTS values of the wires processed by the 5th CH process with routes A, B_c, and C showed 102.7%, 91.0%, 91.5% higher, respectively, compared to that of the initial specimen. The static toughness values of the wires processed by route A were higher than those for other processing routes. From these investigations, it was demonstrated that the CH process, especially route A, could manufacture high-strength low-carbon steel wires with the highest static toughness among the three processing routes.

(2) The compression test indicated that the produced specimen by the CH process buckled when the aspect ratio was larger than 2.6 for all the processing conditions. Therefore, wires produced by the CH process required a careful control of the microstructure and texture evolutions to achieve sufficient workability for various industrial applications. In this study, it was concluded that the aspect ratio of the produced low-carbon steel wires by the multi-pass CH process with an intersecting angle of 130° should be selected smaller than 2.4 to guarantee safe workability for industrial applications.

(3) The EBSD results indicated that the average grain size (3.02 μm) of the specimen produced by the CH process with route C was smaller than those (4.29 μm and 6.71 μm) for the wires produced by routes A and B_c, respectively, for the 5th pass. In addition, the TEM results indicated that the specimen produced by route C showed the smallest deformation bands (less than 1 μm) among the various processing routes. From these microstructure results, it was found that the CH process can be effective in producing fine-grained wires. In particular, the process with route C could manufacture the smallest grains among three processing routes.

(4) The PF and ODF results indicate that the wires produced by the CH process showed mixed texture evolution of shear texture by the ECAP and drawing texture by the wire drawing. The specimens processed by routes A and C up to the 5th pass showed similar deformation texture. The texture intensity of the specimen did not regularly change during the multi-pass process. An increase of simple shear texture intensity was rarely observed during the process due to integrated deformation mode of the rolling, ECAP, and wire drawing processes.

In conclusion, the present work indicated that the processing routes of the CH process could dominantly affect the microstructure and texture evolutions, resulting in mechanical properties and workability changes. Therefore, careful control of the processing routes during the multi-pass CH process is required to obtain proper mechanical properties and workability.

ACKNOWLEDGMENTS

The research grant from POSCO and KITECH was very much appreciated.

REFERENCES

1. Y. Song, W. Wang, D. Gao, E. Y. Yoon, D. J. Lee, and H. S. Kim, *Met. Mater. Int.* **20**, 445 (2014).

2. B. Chen, C. Lu, D. Lin, and X. Zeng, *Met. Mater. Int.* **20**, 285 (2014).
3. C. C. Hsieh, M. S. Shi, and W. Wu, *Met. Mater. Int.* **18**, 1 (2012).
4. G. N. Hadi, N. A. Mahmoud, M. Arya, and Z. Cyrus, *Met. Mater. Int.* **20**, 1 (2014).
5. K. Hajizadeh and B. Eghbali, *Met. Mater. Int.* **20**, 343 (2014).
6. H. S. Kim, S. H. Joo, and H. J. Jeong, *Korean J. Met. Mater.* **52**, 87 (2014).
7. K. H. Lee and S. I. Hong, *Korean J. Met. Mater.* **51**, 621 (2013).
8. U. Chakkingal, A. B. Suriadi, and P. F. Thomson, *Scr. Mater.* **39**, 667 (1998).
9. U. Chakkingal, A. B. Suriadi, and P. F. Thomson, *Mater. Sci. Eng. A* **266**, 241 (1999).
10. J. León and C. J. Luis, *Mater. Sci. Forum* **526**, 19 (2006).
11. S. K. Hwang, Y. G. Jin, I. H. Son, K. H. Rhee, D. L. Lee, and Y. T. Im, *Int. J. Mech. Sci.* **53**, 479 (2011).
12. S. K. Hwang, H. M. Baek, J. W. Lee, I. H. Son, Y. T. Im, and C. M. Bae, *J. Mater. Process. Technol.* **214**, 318 (2014).
13. J. W. Lee, H. M. Baek, S. K. Hwang, I. H. Son, C. M. Bae, and Y. T. Im, *Mater. Des.* **55**, 898 (2014).
14. S. K. Hwang, Y. G. Jin, H. M. Baek, D. K. Kim, I. H. Son, and Y. T. Im, *Steel Res. Int.* Special Edition: ICTP 2011, 314 (2011).
15. S. K. Hwang, H. M. Baek, I. H, Son, Y. T. Im, and C. M. Bae, *Mater. Sci. Eng. A* **579**, 118 (2013).
16. J. H. Kim, S. K. Hwang, Y. T. Im, I. H. Son, and C. M. Bae, *Mater. Sci. Eng. A* **552**, 316 (2012).
17. S. K. Hwang, H. M. Baek, Y. T. Im, I. H. Son, C. M. Bae, and H. W. Lee, *J. Mater. Process. Technol.* **214**, 1398 (2014).
18. Y. Ito and Z. Horita, *Mater. Sci. Eng. A* **503**, 32 (2009).
19. Sugondo, J. A. Szpunar, and P. Gangli, *J. Mater. Process. Technol.* **16**, 305 (1991).
20. V. M. Segal, V. I. Reznikov, A. E. Drobyshevskii, and V. I. Kopylov, *Izvestia Akademii nauk SSSR. Metally* **1**, 115 (1981).
21. M. Furukawa, Y. Iwahashi, Z. Horita, M. Nemoto, and T. G. Langdon, *Mater. Sci. Eng. A* **257**, 328 (1998).
22. J. S. Choi, Y. G. Jin, H. C. Lee, and Y. T. Im, *Mater. Trans.* **52**, 173 (2011).
23. J. S. Choi, S. Nawaz, S. K. Hwang, H. C. Lee, and Y. T. Im, *Int. J. Mech. Sci.* **52**, 1269 (2010).
24. ASTM Committee E28.04, *E8M-04: Standard Test Methods for Tension Testing of Metallic Materials*. ASTM International, West Conshohocken (2006).
25. Y. Fukuda, K. Oh-ishi, Z. Horita, and T. G. Langdon, *Acta Mater.* **50**, 1359 (2002).
26. S. Li, X. Li, and L. Yang, *Acta Mater.* **61**, 4398 (2013).
27. P. B. Prangnell, A. Gholinia, and V. M. Markushev, *Proceedings of the NATO Advanced Research Workshop on Investigation and Applications of Severe Plastic Deformation* (Eds. T. C. Lowe and R. Z. Valiev), p.65, Kluwer Academic Publisher, Moscow, Russia (1999).
28. T. G. Langdon, M. Furukawa, M. Nemoto, Z. Horita, and J. Organomet, *Chem*. **52**, 30 (2000).
29. Y. T. Zhu and T. C. Lowe, *Mater. Sci. Eng. A* **291**, 46 (2000).